International Journal of Mass Spectrometry 408 (2016) 62–76

Contents lists available at ScienceDirect

International Journal of Mass Spectrometry

journal homepage: www.elsevier.com/locate/ijms

Determination of multipole coefficients in toroidal ion trap mass analysers

Appala Naidu Kotana [a], Atanu K. Mohanty [a,b,*]

[a] Department of Computational and Data Sciences, Indian Institute of Science, Bangalore 560012, India
[b] Department of Instrumentation and Applied Physics, Indian Institute of Science, Bangalore 560012, India

ARTICLE INFO

Article history:
Received 6 May 2016
Received in revised form 28 June 2016
Accepted 29 June 2016
Available online 4 August 2016

Keywords:
Toroidal ion trap
Mathieu parameters
Secular frequency
Toroidal harmonics
Toroidal multipole coefficients

ABSTRACT

In this paper, we present methods to determine multipole coefficients for describing the potential in toroidal ion trap mass analysers. Three different methods have been presented to compute the toroidal multipole coefficients. The first method uses at least square fit (LS) and is useful when we have ability to compute potential at a set of points in the trapping region. In the second method we use the Discrete Fourier Transform (DFT) of potentials on a circle in the trapping region. The third method uses surface charge distribution obtained from the Boundary Element Method (BEM) to compute these coefficients. Using these multipole coefficients we have presented (1) equations of ion motion in toroidal ion traps, (2) the Mathieu parameters in terms of multipole coefficients and (3) the secular frequency of ion motion in these traps. It has been shown that the secular frequency obtained from our method has a good match with that obtained from numerical trajectory simulation.

1. Introduction

In this paper, we discuss three different methods to determine multipole coefficients suitable for describing the potential in toroidal ion trap mass analysers.

A toroidal ion trap mass analyser can be viewed as a linear ion trap curved around and connected at the ends or as a cross section of a quadrupole ion trap (QIT) rotated on edge to form the toroid [5,13]. This produces a circular ion trapping region [4]. These are axi-symmetric devices. In the literature the toroidal ion trap was originally presented as a storage device [2,3]. Later, the use of toroidal ion traps as mass analysers was demonstrated by Bier and Syka [4] and Lammert et al. [5]. These analysers have large trapping region and less space charge effect in comparison to quadrupole ion trap mass analysers in which trapping occurs at a point [4]. These analysers are now available commercially in a miniaturized structure [36].

Toroidal ion trap mass analysers have received the attention of several researchers [6–15]. These studies include design and simplification of toroidal ion trap mass analysers [5–10] and miniaturization of toroidal mass analysers [6,11–13]. Another direction to this investigation were simulation studies of ion trajectories in toroidal ion trap mass analysers [7,8].

Efforts to optimize the performance of toroidal ion trap mass analysers require the evaluation of potentials and fields within the device. Lammert et al. [5] have made toroidal ion trap mass analyser by optimizing the electric field obtained numerically. Taylor and Austin [10] have designed a simplified and optimized toroidal ion trap geometry by setting desired percentage of multipole coefficients. These multipole coefficients are obtained by polynomial fitting to the numerically obtained potential along its axis. This is same as multipole expansion in axially symmetric ion trap mass analysers such as QIT, in which potential around trapping point is expressed in series form of Legendre polynomials [30,16,18]. Higgs and Austin [7] have taken a polynomial fit to the numerically obtained potential in the trapping region of the toroidal ion trap and have used this polynomial to compute the trajectory of ion motion.

Some shortcomings of these approaches have been highlighted in the literature. For instance Higgs and Austin [7] pointed out that there is a lack of understanding of higher order field contributions and their effects on ion motion in toroidal ion traps. Further, Higgs et al. [8] suggested that a solution based on a toroidal coordinate system may be more appropriate and useful. It is at this point that our study hopes to contribute. We will take up for investigation the determination of multipole coefficients in the toroidal coordinate system. Such studies are not available in the mass spectrometry

* Corresponding author.
E-mail addresses: appala@grads.cds.iisc.ac.in (A.N. Kotana), amohanty@cds.iisc.ac.in (A.K. Mohanty).

http://dx.doi.org/10.1016/j.ijms.2016.06.011
1387-3806/

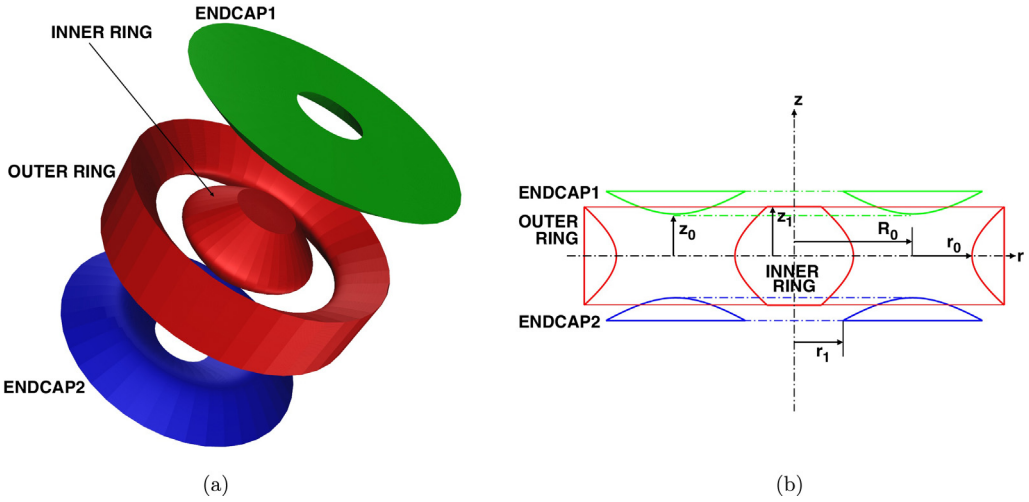

Fig. 1. Schematic view of HypTorTrap obtained from a quadrupole ion trap rotated on edge to form the toroid. (a) Three dimensional view and (b) cross section in *xz*-plane.

literature and to our knowledge it is not readily available in the mathematical literature too.

Three approaches have been adopted in this study for three different circumstances. In the first method, a least square fit is used. This method is useful when we have ability to compute potential at a set of points in the trapping region. We call this method as LS method in this paper. This method is analogous to the method used to compute multipole coefficients for cylindrical ion traps (CIT) by Wu et al. [18], in which a least square fit of potential with polynomial has been used. In the second method, we use Discrete Fourier Transform (DFT) of potential on a circle (having a particular property which will be discussed later) in the trapping region. This method has greater accuracy with less computational effort, in comparison to the LS method. We call this method as the DFT method in our discussion. This method is analogous to computation of Laurent coefficients using the DFT [27]. The third method is used when the surface charge distribution has been determined using the boundary element method. We call this method as the Surface Charge BEM (SC-BEM) method. This method is analogous to the method used by Beaty [30] to compute multipole coefficients for the QIT.

Having obtained toroidal multipole coefficients, the Mathieu parameters [1] will be shown in terms of these coefficients. Although the formulae for Mathieu parameters in terms of multipole coefficients for nonlinear ion traps, such as CIT, have been presented in the literature [17], similar formulae do not exist for toroidal ion traps. Having obtained the Mathieu parameters in terms of toroidal multipole coefficients, we will show how these can be used to estimate secular frequencies [1] in these traps.

Five separate toroidal trap geometries have been taken up for investigation. Of these, two are similar to the geometries reported in the literature, while the other three are chosen to demonstrate that our method can handle the variety of complexities that may arise. However, the methods presented in this paper are applicable to toroidal ion traps in general, and not restricted to the example geometries discussed here.

Geometries considered in the study are presented in Section 2, and Section 3 presents the computational methods. Required theory will be discussed in Section 4 and results are presented in Section 5.

2. Geometries considered

In this section we present five geometries that have been taken up for investigation.

2.1. The geometry HypTorTrap

The first geometry considered will be referred to as HypTorTrap. This geometry has four electrodes, each electrode cross section is hyperbolic. This geometry is similar to the symmetric version of the geometry considered by Lammert et al. [5]. We have considered this for simplicity, although the asymmetric version that they have investigated has better performance than the symmetric one. Fig. 1(a) shows its three dimensional view. This trap is obtained from QIT rotated on edge to form the toroid. Its cross section in *xz*-plane is shown in Fig. 1(b). The distance R_0, from origin to the mid point between ring electrodes on *x*-axis is 20 mm. The half distance r_0, between ring electrodes is taken as 10 mm and the half distance z_0, between endcap electrodes is taken as 7.07 mm. The truncation of ring electrodes as well as endcap electrodes is done such that the trap has top bottom symmetry. The truncation of endcap electrodes are done such that the least distance between *z*-axis and truncation point is r_1, which is taken as 8.24 mm. The ring electrodes are truncated at height z_1 from radial plane (or *xy*-plane) and is taken as 8.31 mm.

The parametric equations of the hyperbolic surfaces are given as follows: INNER RING: $r(t) = R_0 - r_0 \cosh(t)$ and $z(t) = z_0 \sinh(t)$; OUTER RING: $r(t) = R_0 + r_0 \cosh(t)$ and $z(t) = z_0 \sinh(t)$; ENDCAP1: $r(t) = R_0 + r_0 \sinh(t)$ and $z(t) = z_0 \cosh(t)$; ENDCAP2: $r(t) = R_0 + r_0 \sinh(t)$ and $z(t) = -z_0 \cosh(t)$. In all cases t changes from -1 to 1.

2.2. The geometry CylTorTrap

The second geometry considered will be referred to as CylTorTrap. It is obtained by replacing hyperbolic electrodes of the trap shown in Fig. 1(a), with flat electrodes. This too, like HypTorTrap discussed above, is a symmetric version of the trap reported by Lammert et al. [10]. Fig. 2(a) shows its three dimensional view. The electrodes are obtained by replacing hyperbolic surfaces of ring electrodes shown in Fig. 1(a) with cylinders and endcap electrodes with annuli. Its cross section in *xz*-plane is shown in Fig. 2(b). The distance R_0, from origin to the mid point between concentric cylinders on *x*-axis is 20 mm. The half distance r_0, between concentric cylinders is taken as 10 mm and the half distance z_0, between endcap electrodes is taken as 10 mm. The half height z_1, of cylinders forming ring electrodes is taken as 6 mm. The thickness d, of cylinders forming ring electrodes is taken as 4 mm. The hole radius r_1, of annuli forming endcap electrodes is taken as 6 mm. The thickness d, of annuli forming endcap electrodes is taken as 4 mm.

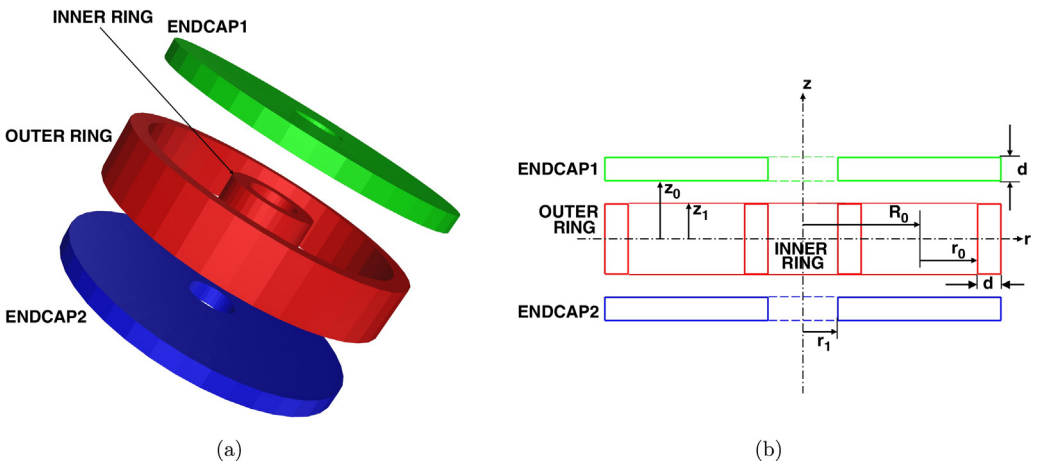

(a) (b)

Fig. 2. Schematic view of CylTorTrap obtained by replacing hyperbolic surfaces of ring electrodes shown in 1(a) with cylinders and endcap electrodes with annuli. (a) Three dimensional view and (b) cross section in *xz*-plane.

2.3. The geometry CircRodTorTrap0

The third geometry considered will be referred to as CircRodTorTrap0. It is obtained by replacing all hyperbolic electrodes of the trap shown in Fig. 1(a), with circular rod shaped electrodes. Fig. 3(a) shows its three dimensional view. The geometry is formed such that the centers of ring electrodes in *xz*-plane lie on the *x*-axis and the line joining centers of endcap electrodes is perpendicular to the *x*-axis. Its cross section in *xz*-plane is shown in Fig. 3(b). The diameter *d*, of the rods are taken as 20 mm. The distance R_0, from origin to the mid point of centers of ring electrode rods is taken as 40 mm. The half distance r_0, between ring electrodes and the half distance z_0, between endcap electrodes are taken as 20 mm.

2.4. The geometry CircRodTorTrap30

The fourth geometry considered will be referred to as CircRodTorTrap30. It is obtained by replacing all hyperbolic electrodes of the trap shown in Fig. 1(a), with circular rod shaped electrodes. Fig. 4(a) shows its three dimensional view. The geometry is formed such that the line joining centers of ring electrodes in *xz*-plane subtends 30° with radial plane and the line joining centers of endcap electrodes is perpendicular to the line joining centers of ring electrodes. Its cross section in *xz*-plane is shown in Fig. 4(b). The diameter *d*, of the rods are taken as 20 mm. The distance R_0, from origin to the mid point of centers of ring electrode rods is taken as 40 mm. The half distance r_0, between ring electrodes and the half distance z_0, between endcap electrodes are taken as 20 mm.

2.5. The geometry CircRodTorTrap45

The fifth geometry considered will be referred to as CircRodTorTrap45. It is obtained by replacing all hyperbolic electrodes of the trap shown in Fig. 1(a), with circular rod shaped electrodes. Fig. 5(a) shows its three dimensional view. The geometry is formed such that the line joining centers of ring electrodes in *xz*-plane subtends 45° with radial plane and the line joining centers of endcap electrodes is perpendicular to the line joining centers of ring electrodes. Its cross section in *xz*-plane is shown in Fig. 5(b). The diameter *d*, of the rods are taken as 20 mm. The distance R_0, from origin to the mid point of centers of ring electrode rods is taken as 40 mm. The

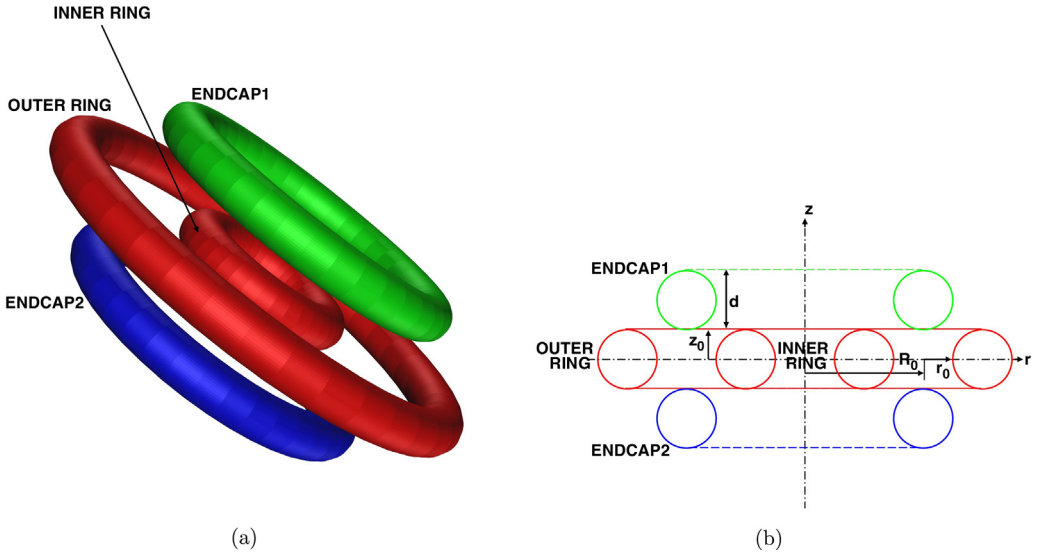

(a) (b)

Fig. 3. Schematic view of CircRodTorTrap0 obtained by replacing all hyperbolic electrodes of the trap shown in Fig. 1(a), with circular rod shaped electrodes. The centers of ring electrodes in *xz*-plane lie on the *x*-axis and the line joining centers of endcap electrodes is perpendicular to the *x*-axis. (a) Three dimensional view and (b) cross section in *xz*-plane.

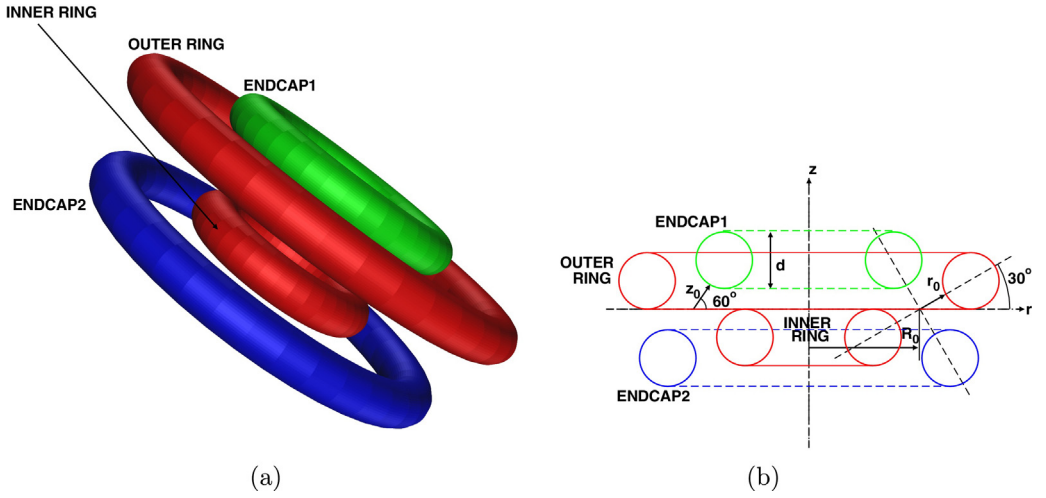

Fig. 4. Schematic view of CircRodTorTrap30 obtained by replacing all hyperbolic electrodes of the trap shown in Fig. 1(a), with circular rod shaped electrodes. The line joining centers of ring electrodes in *xz*-plane subtends 30° with radial plane and the line joining centers of endcap electrodes is perpendicular to the line joining centers of ring electrodes. (a) Three dimensional view and (b) cross section in *xz*-plane.

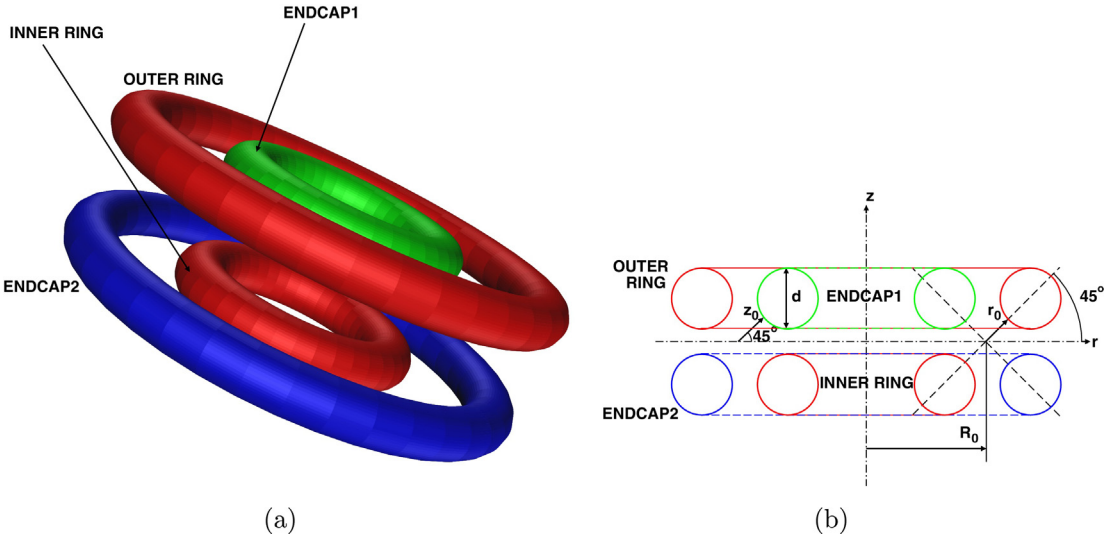

Fig. 5. Schematic view of CircRodTorTrap45 obtained by replacing all hyperbolic electrodes of the trap shown in Fig. 1(a), with circular rod shaped electrodes. The line joining centers of ring electrodes in *xz*-plane subtends 45° with radial plane and the line joining centers of endcap electrodes is perpendicular to the line joining centers of ring electrodes. (a) Three dimensional view and (b) cross section in *xz*-plane.

Table 1
Trap parameters (all dimensions are in millimeters). θ, the angle between the line joining the centers of the two ring electrodes with the *xy*-plane, is in degrees.

TRAP	R_0	r_0	z_0	r_1	z_1	d	θ (in degrees)
HypTorTrap	20	10	7.07	8.24	8.31	–	–
CylTorTrap	20	10	10	6	6	4	–
CircRodTorTrap0	40	20	20	–	–	20	0
CircRodTorTrap30	40	20	20	–	–	20	30
CircRodTorTrap45	40	20	20	–	–	20	45

half distance r_0, between ring electrodes and the half distance z_0, between endcap electrodes are taken as 20 mm.

The dimensions of the traps that have been used in our simulations are tabulated in Table 1 for easy reference.

3. Numerical methods

In this section we discuss the boundary element method which has been used to calculate charge distribution on surfaces of electrodes of ion trap. We also present a discussion on trajectory computation and also the method we have adopted to obtain frequencies from trajectory. Finally we present the methods used for the computation of associated Legendre functions.

3.1. Boundary element method, least square solution and the DFT

We use Boundary Element Method (BEM) to calculate charge distribution on the surfaces of the electrodes of ion traps. We use the same method followed by Tallapragada et al. [16] to obtain the elemental ring charges which describe the surface charge distribution on the electrodes. Potential and electric field are obtained from these elemental ring charges.

For obtaining the least square solutions and the DFT we have used appropriate routines available in Octave [44].

3.2. Computation of trajectory and frequencies

The equation of motion of an ion in the ion trap is obtained from Newton's second law. The trajectory is computed by solving this equation of motion. The equation of motion depend on the

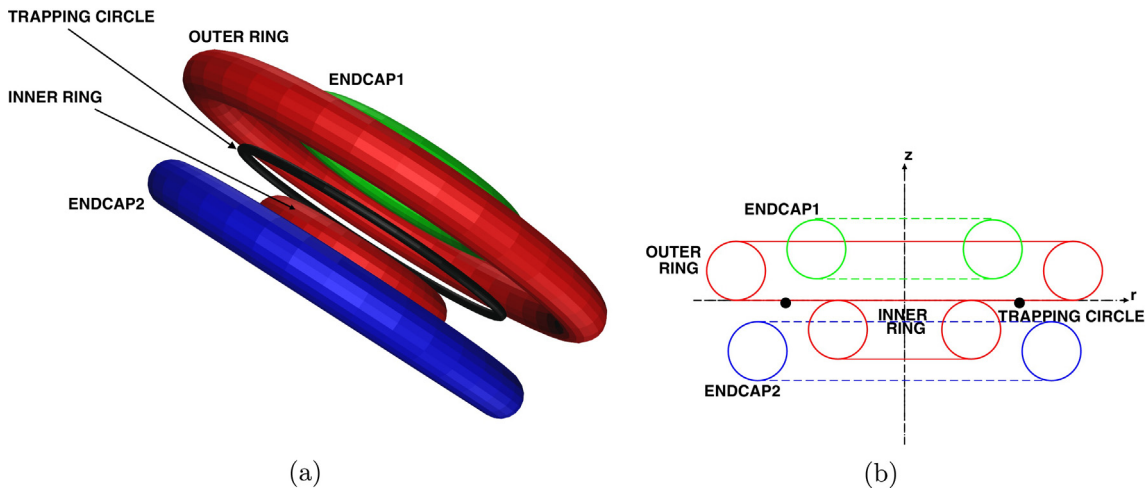

Fig. 6. Schematic view of toroidal trap (CircRodTorTrap30 shown in Fig. 4) with trapping circle. (a) Three dimensional view and (b) cross section in *xz*-plane. The trapping circle is shown as a black circle in three dimensional view and as two black dots in the cross sectional view.

nature of the electric field in the trap and since these fields are non linear, they do not have closed form solution. In view of this we use numerical methods to compute trajectory. In our present study we use Runge-Kutta fourth order method [24,25]. The frequencies present in ion trajectory are obtained using an open source package "harminv" [43].

3.3. Determination of the trapping circle

In this section we outline a method for determining the coordinates of the trapping circle. For the analysis carried out in this paper, the focal circle that will be defined in Section 4, will be this trapping circle.

In general, there are no closed form solutions to obtain the trapping circle. It needs to be determined numerically by locating the point on the *xz*-plane where the field is zero. We have adopted the Newton method [24,37]. In the Newton method, we find the Jacobian matrix using a central difference scheme with step size 10^{-8}. Of the point so determined, the *x*-coordinate is the radius of the trapping circle and will be indicated by the symbol a and the *z*-coordinate will be indicated by the symbol z_c in the derivations below.

In the toroidal coordinate system points are referenced with respect to the focal circle (Fig. 7). In cases where this circle is not on the *xy*-plane ($z_c \neq 0$) an appropriate shift in *z* is carried out to define the toroidal coordinates.

Even in traps where the cross section of the ring and endcap electrodes appears to have a geometric center, examples from our study being CylTorTrap, CircRodTorTrap0, CircRodTorTrap30, CircRodTorTrap45 but not HypTorTrap, the trapping circle may not pass through this geometric center. For example, the geometric center of the electrodes in case of CircRodTorTrap30 is on the *xy*-plane, but the trapping circle is *not*, as will be seen later.

An interesting perspective for this phenomenon, that the geometric center and the trapping center do not coincide, was provided to us succinctly by an anonymous reviewer of this manuscript. We quote, "The origin of this effect is that points on the cross section will create a larger surface of revolution the farther away they are from the rotational axis. In other words, the outer ring electrode has a stronger effect on the trapping potential than the inner ring, and the outer ring pushes the trapping center inward. For traps without top-bottom symmetry, the outer electrodes push inward and upward (or downward), resulting in a saddle point that is off from the center of the cross section."

In order to identify the location of the trapping circle we consider, as an example, CircRodTorTrap30, a trap with no top-bottom symmetry. The schematic view of this trap is shown in Fig. 6. The trapping circle is seen as a black circle in three dimensional view (Fig. 6(a)) and as two black dots in cross sectional view (Fig. 6(b)). The black circle in Fig. 6(a) is referred to trapping circle. Its offset from the *xy*-plane may be more clearly seen in Fig. 6(b).

3.4. Associated Legendre functions computation

In order to obtain toroidal multipole coefficients, computation of associated Legendre functions of fractional order is required. We have used recurrence relation for the computation of associated Legendre functions of first kind [38] and Legendre functions of second kind are computed using algorithm proposed by Fettis [22].

4. Theory

The method for representing the potential in terms of Legendre polynomials is useful for axially symmetric ion traps such as the CIT, in which trapping happens at a point. In Linear Ion Traps, where trapping occurs along a line and not at a point, there is no axial symmetry [4,34]. Here trigonometric functions are used to describe the potential inside the trap [34,35]. For the toroidal ion trap, although there is axial symmetry, the trapping is localized on a circle and not at a point. Here an expansion based on toroidal harmonics is appropriate [8].

In this section, first we discuss how to denote the potential in toroidal coordinate system. This is followed by three methods that we have developed to evaluate toroidal multipole coefficients. Finally, we present the Mathieu parameters in terms of toroidal multipole coefficients.

4.1. Potential inside toroidal ion trap in toroidal coordinates

A schematic view of the representation of coordinates in the toroidal coordinate system [19,45] is shown in Fig. 7. An arbitrary point *P* is denoted by (σ, τ, ϕ). The circle shown in this figure is the focal circle and it is taken on the *xy*-plane. The line passing through origin and the projection of point *P* on the *xy*-plane intersects this circle at two different points. Of these, the longest distance point from *P* is called F_1 and the distance PF_1 is defined as d_1. The shortest distance point from *P* is called F_2 and the distance PF_2 is defined as

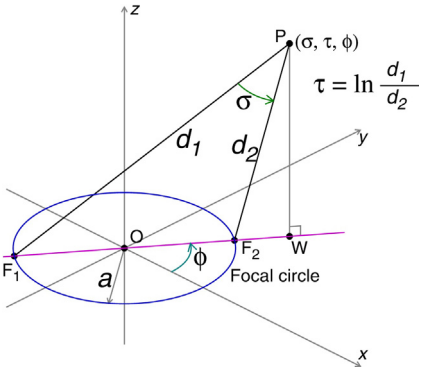

Fig. 7. Toroidal coordinate system. x, y, z are Cartesian coordinates, O is the origin, W is the projection of the point P on the xy-plane.

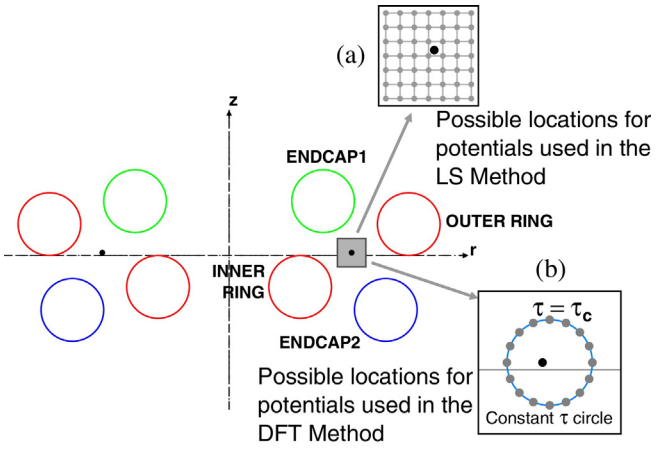

Fig. 8. The cross sectional view of an example toroidal ion trap indicating the region in which the potential is required for computing the multipole coefficients. (a) Magnified view of the grid used for the LS method, (b) magnified view of the constant τ circle for the DFT method.

d_2. The parameter τ is defined as $\log\left(\frac{d_1}{d_2}\right)$ and its range is from 0 to ∞. σ is defined by an angle between PF_1 and PF_2 in the range 0 to 2π. σ varies from 0 to π for positive values of z and from π to 2π when z is negative. The angle ϕ is defined to be angle subtended with x-axis by the line joining origin and projection of P in xy-plane. It is in the range 0 to 2π. The length a shown in Fig. 7 is radius of the focal circle. The toroidal coordinates and Cartesian coordinates are related by $x = a\frac{\sinh\tau}{\cosh\tau-\cos\sigma}\cos\phi$, $y = a\frac{\sinh\tau}{\cosh\tau-\cos\sigma}\sin\phi$ and $z = a\frac{\sin\sigma}{\cosh\tau-\cos\sigma}$ [19]. We remind the reader that when the focal circle is not on the xy-plane, z should be replaced by $z - z_c$, z_c being the offset of the focal circle determined by the method outlined in Section 3.3.

An axially symmetric separable solution for the Laplace equation in the toroidal coordinates is [19,20]

$$\sqrt{\cosh\tau-\cos\sigma}[a_\nu\cos(\nu\sigma)+b_\nu\sin(\nu\sigma)][c_\nu P_{\nu-\frac{1}{2}}(\cosh\tau) + d_\nu Q_{\nu-\frac{1}{2}}(\cosh\tau)]$$

where ν is an integer; a_ν, b_ν, c_ν and d_ν are constants; $P_{\nu-\frac{1}{2}}$ and $Q_{\nu-\frac{1}{2}}$ are associated Legendre functions of the first and the second kind respectively. As we approach trapping circle $\tau\to\infty$. The functions $\sqrt{\cosh\tau-\cos\sigma}P_{\nu-\frac{1}{2}}(\cosh\tau)\to\infty$ as $\tau\to\infty$. That is, near the trapping circle these functions are unbounded. Hence these are discarded in the general form of the potential for toroidal ion traps. Hence, a suitable expansion for the potential near the trapping circle is [19,20]

$$\Psi(\sigma,\tau) = a_0\sqrt{\cosh\tau-\cos\sigma}\,Q_{-\frac{1}{2}}(\cosh\tau)+\sqrt{\cosh\tau-\cos\sigma} \times\sum_{\nu=1}^{\infty}[a_\nu\cos(\nu\sigma)+b_\nu\sin(\nu\sigma)]Q_{\nu-\frac{1}{2}}(\cosh\tau) \quad (1)$$

or

$$\Psi(\sigma,\tau) = a_0T_0(\sigma,\tau)+\sum_{\nu=1}^{\infty}[a_\nu T_\nu(\sigma,\tau)+b_\nu U_\nu(\sigma,\tau)] \quad (2)$$

where $\Psi(\sigma,\tau)$ is potential at the point (σ,τ) and $Q_{\nu-\frac{1}{2}}(.)$ are associated Legendre functions of second kind [20]. a_ν and b_ν are constants to be found from given boundary conditions. $T_\nu(\sigma,\tau)$ is a toroidal even harmonic, $U_\nu(\sigma,\tau)$ is a toroidal odd harmonic and they are defined as

$$T_\nu(\sigma,\tau) = \sqrt{\cosh\tau-\cos\sigma}\cos(\nu\sigma)Q_{\nu-\frac{1}{2}}(\cosh\tau), \quad (3)$$

$$U_\nu(\sigma,\tau) = \sqrt{\cosh\tau-\cos\sigma}\sin(\nu\sigma)Q_{\nu-\frac{1}{2}}(\cosh\tau). \quad (4)$$

The unknowns a_ν and b_ν are called toroidal even and toroidal odd multipole coefficients, respectively [9].

4.2. *Determination of* a_ν *and* b_ν *using least square solution*

This method is useful when we have ability to compute potential in some region within the trapping region. As an example, this region is shown as a square shaded region in Fig. 8. In general this region does not necessarily need to have square geometry. In principle, it could be any region where the potentials are known. For good numerical results, the region so selected should not be too close to the electrodes of the trap. Also, it is desired that the grid chosen should be centered with respect to the trapping center. In order to compute toroidal multipole coefficients a_ν and b_ν, we select a set of n points around trapping center where the potentials have been previously computed numerically (say, by the BEM or finite difference method or finite element method, the last two methods have not been discussed in this paper). We wish to minimize the difference between the computed potentials and the potentials obtained by truncating Eq. (2) to include terms till $\nu = N$ in the least square sense. The error

$$E = \sum_{j=1}^{n}\left(a_0T_0(\sigma_j,\tau_j)+\sum_{\nu=1}^{N}[a_\nu T_\nu(\sigma_j,\tau_j)+b_\nu U_\nu(\sigma_j,\tau_j)]-\psi_j\right)^2 \quad (5)$$

is minimized with respect to $a_0, a_1, \ldots a_N, b_1, b_2, \ldots b_N$. Here ψ_j is potential at (σ_j,τ_j) obtained numerically, $T_\nu(\sigma_j,\tau_j)$ is evaluation of $T_\nu(.)$ at (σ_j,τ_j), $U_\nu(\sigma_j,\tau_j)$ is evaluation of $U_\nu(.)$ at (σ_j,τ_j). Setting $\frac{\partial E}{\partial a_\nu} = 0$, for $\nu = 0, 1 \ldots N$ and $\frac{\partial E}{\partial b_\nu} = 0$, for $\nu = 1, \ldots N$ leads to the matrix equation $M^TM\,X = M^Tb$, where M will be described below. While this can be solved directly, problems arise if M is ill-conditioned. This is because the condition number of M^TM is the square of the condition number of M. A better alternative is to require that

$$MX = b \quad (6)$$

be solved in the least square sense [25,31–33]. This results in orthogonal decomposition such as QR factorization or SVD being

used by Octave or LAPACK. Here M is a matrix of known quantities having size $n \times (2N+1)$ and defined as

$$M = \begin{bmatrix} T_0(\sigma_1,\tau_1) & \dots & T_N(\sigma_1,\tau_1) & U_1(\sigma_1,\tau_1) & \dots & U_N(\sigma_1,\tau_1) \\ T_0(\sigma_2,\tau_2) & \dots & T_N(\sigma_2,\tau_2) & U_1(\sigma_2,\tau_2) & \dots & U_N(\sigma_2,\tau_2) \\ \vdots & & \vdots & \vdots & & \vdots \\ \vdots & & \vdots & \vdots & & \vdots \\ T_0(\sigma_n,\tau_n) & \dots & T_N(\sigma_n,\tau_n) & U_1(\sigma_n,\tau_n) & \dots & U_N(\sigma_n,\tau_n) \end{bmatrix}.$$

X is a column vector of unknowns having length $2N+1$ and defined as

$$X = \begin{bmatrix} a_0 & a_1 & \dots & a_N & b_1 & \dots & b_N \end{bmatrix}^T$$

and b is a column vector of potentials of length n and defined as

$$b = \begin{bmatrix} \psi_1 & \psi_2 & \dots & \dots & \psi_n \end{bmatrix}^T.$$

The number of points n, should be chosen larger than the number of unknowns $2N+1$. The least square solution X of Eq. (6) provides a_ν's and b_ν's. We call this method as the LS method.

4.3. Determination of a_ν and b_ν using Discrete Fourier Transform (DFT)

This method is useful when we have ability to compute potential on a circle with constant τ. A schematic view of this circle is shown (with label $\tau = \tau_c$) in Fig. 8 on which we computed potentials for this method. This method has greater accuracy and requires less computational effort, in comparison to the LS method. From Eq. (1) we see that

$$\frac{\Psi(\sigma,\tau)}{\sqrt{\cosh\tau - \cos\sigma}} = a_0 Q_{-\frac{1}{2}}(\cosh\tau) + \sum_{\nu=1}^{\infty}[a_\nu \cos(\nu\sigma) + b_\nu \sin(\nu\sigma)]Q_{\nu-\frac{1}{2}}(\cosh\tau) \quad (7)$$

is in the form of a Fourier series in σ, in which the coefficients a_ν and b_ν are multiplied by $Q_{\nu-\frac{1}{2}}(\cosh\tau)$. Although the Fourier coefficients could be computed by the Euler formulae, a faster alternative is to compute the DFT using the FFT algorithm. Because of this, it is convenient to use the complex form of the Fourier series. If we use a fixed τ, say $\tau = \tau_c$, then we define a function $g(\sigma)$ given by

$$g(\sigma) = \frac{\Psi(\sigma,\tau_c)}{\sqrt{\cosh\tau_c - \cos\sigma}} = \alpha_0 + \sum_{\nu=1}^{\infty}[\alpha_\nu \cos(\nu\sigma) + \beta_\nu \sin(\nu\sigma)] = \sum_{\nu=-\infty}^{\infty} \hat{g}(\nu) e^{i\nu\sigma} \quad (8)$$

where

$$\alpha_\nu = a_\nu Q_{\nu-\frac{1}{2}}(\cosh\tau_c), \quad \nu = 0, a, 2\dots \quad (9)$$

and

$$\beta_\nu = b_\nu Q_{\nu-\frac{1}{2}}(\cosh\tau_c), \quad \nu = 1, b, 3\dots \quad (10)$$

Here α_ν and β_ν are real Fourier coefficients, $\hat{g}(\nu)$ are complex Fourier coefficients of the function $g(\sigma)$. a_ν and b_ν are the toroidal multipole coefficients that we seek. The function $g(\sigma)$ depends on the potential $\Psi(\sigma,\tau_c)$, which may be computed by different methods such as the finite difference method, the finite element method or the boundary element method. The real Fourier coefficients α_ν and β_ν are related to complex Fourier coefficients by

$$\alpha_0 = \hat{g}(0) \quad (11)$$

and for positive integer ν

$$\alpha_\nu = 2\Re\{\hat{g}(\nu)\} \quad (12)$$

$$\beta_\nu = -2\Im\{\hat{g}(\nu)\} \quad (13)$$

where $\Re\{\hat{g}(\nu)\}$ denotes real part and $\Im\{\hat{g}(\nu)\}$ denotes the imaginary part of $\hat{g}(\nu)$. In order to compute the DFT, we require the finite length sequence $g_k = g(\sigma_k)$ for $\sigma_k = \frac{k2\pi}{N_s}$, $k = 0, 1, 2\dots N_s - 1$ with N_s being power of 2. Let G_ν, ($\nu = 0, 1, 2\dots N_s - 1$) be DFT (obtained using the FFT) [26,28] of this finite length sequence. The relationship between G_ν and the complex Fourier coefficients $\hat{g}(\nu)$ is given by [26,28]

$$\frac{G_\nu}{N_s} = \sum_{\nu=-\infty}^{\infty} \hat{g}(\nu + mN_s). \quad (14)$$

This shows that $\hat{g}(\nu)$ is aliased [28] with higher index coefficients such as $\hat{g}(\nu + N_s)$, $\hat{g}(\nu - N_s)$, $\hat{g}(\nu + 2N_s)$, $\hat{g}(\nu - 2N_s)\dots$. But if N_s is made sufficiently large, these higher index coefficients become small so that the aliasing error is negligible. Then we use

$$\hat{g}(\nu) = \frac{G_\nu}{N_s} \quad (15)$$

for ν small compared to N_s with negligible aliasing error. It is now possible to obtain a_ν, b_ν by

$$a_\nu = \frac{\alpha_\nu}{Q_{\nu-\frac{1}{2}}(\cosh\tau_c)} \quad (16)$$

$$b_\nu = \frac{\beta_\nu}{Q_{\nu-\frac{1}{2}}(\cosh\tau_c)} \quad (17)$$

where α_ν and β_ν are obtained from $\hat{g}(\nu)$ using Eqs. (11)–(13). We call this method as the DFT method. We point out that in this method the potentials are required at several points on a constant τ circle. Although for these points the σ values are equispaced, the points are not spaced uniformly on the circle. Also, these points need not coincide with the grid points in the finite difference (FDM) and the finite element (FEM) methods. Because of this, when FDM or FEM is used, there is a need to compute the potentials required at these points by appropriate interpolation techniques.

4.4. Determination of a_ν and b_ν from the elemental ring charges determined by the BEM

The BEM described by Tallapragada et al. [16] provides a method to obtain the elemental ring charges which define the charge distribution on the surface of the trap electrodes. In this section, we outline a method to determine the toroidal multipole coefficients from these elemental ring charges. We first determine the potential due to a single ring charge as a toroidal multipole expansion in the vicinity of the trapping circle. This allows the contribution of a single ring charge to any toroidal multipole coefficient to be calculated. By summing the contribution from all the ring charges obtained from the BEM we finally compute the desired toroidal multipole coefficients. A schematic view of charged ring (blue circle) and trapping circle (dotted black circle) is shown in Fig. 9. Let $\frac{q_{\text{ring},j} d\phi_j}{2\pi}$ be an elemental charge (shown in green) located at point $(\sigma_j, \tau_j, \phi_j)$ on the ring as shown in Fig. 9. Here $q_{\text{ring},j}$ is total charge on the ring and $d\phi_j$ is the angle subtended at origin by the projection

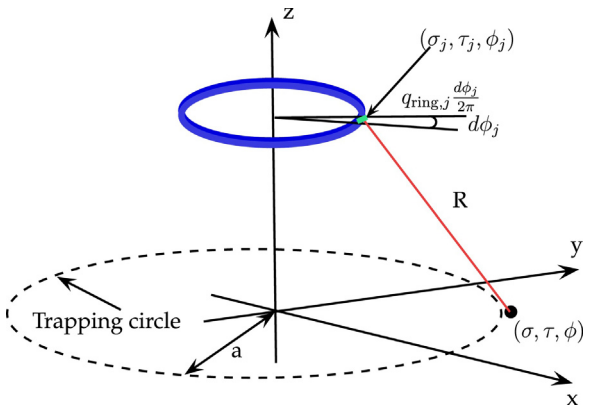

Fig. 9. Potential due to ring charge.

of elemental charge in the *xy*-plane. Then the potential due to this elemental charge at a point (σ, τ, ϕ) is given by

$$\psi_{\text{elem}}(\sigma, \tau, \phi) = \frac{1}{4\pi\varepsilon_0}\frac{q_{\text{ring},j}d\phi_j}{2\pi}\frac{1}{R} \tag{18}$$

where ε_0 is permittivity constant and R is distance between (σ, τ, ϕ) and $(\sigma_j, \tau_j, \phi_j)$. The expansion of $\frac{1}{R}$ in terms of toroidal coordinates [20,21] is given by

$$\frac{1}{R} = \frac{1}{\pi a}\sqrt{(\cosh\tau - \cos\sigma)(\cosh\tau_j - \cos\sigma_j)} \times \sum_{\mu=0}^{\infty}\sum_{\nu=0}^{\infty}\epsilon_\mu\epsilon_\nu(-i)^\mu\frac{\Gamma(\nu+\mu-\frac{1}{2})}{\Gamma(\nu-\mu-\frac{1}{2})}\left[\cos(\mu(\phi-\phi_j)) \times \cos(\nu(\sigma-\sigma_j))\right]\begin{cases} P^\mu_{\nu-\frac{1}{2}}(\cosh\tau)Q^\mu_{\nu-\frac{1}{2}}(\cosh\tau_j); & \tau_j > \tau \\ P^\mu_{\nu-\frac{1}{2}}(\cosh\tau_j)Q^\mu_{\nu-\frac{1}{2}}(\cosh\tau); & \tau_j < \tau \end{cases} \tag{19}$$

where a is radius of the focal circle, ϵ_ν is Neumann factor [20], its value is 1 when $\nu = 0$ and 2 for $\nu > 0$. $\Gamma(.)$ is gamma function, $P^\mu_{\nu-\frac{1}{2}}(.)$ are associated Legendre functions of first kind, $Q^\mu_{\nu-\frac{1}{2}}(.)$ are associated Legendre functions of second kind. We discard μ in notation when it is zero. The series form of $\frac{1}{R}$ is taken from Eq. (19) by assuming $\tau > \tau_j$, as the point (σ, τ, ϕ) is in the vicinity of the trapping circle. Substituting $\frac{1}{R}$ in Eq. (18) and integrating with respect to ϕ_j will give potential (independent of both ϕ and ϕ_j) due to ring charge as follows

$$\psi_r(\sigma, \tau) = \frac{q_{\text{ring},j}}{4\pi\varepsilon_0}\frac{1}{\pi a}\sqrt{(\cosh\tau - \cos\sigma)(\cosh\tau_j - \cos\sigma_j)} \times \sum_{\nu=0}^{\infty}\epsilon_\nu\cos(\nu(\sigma-\sigma_j))P_{\nu-\frac{1}{2}}(\cosh\tau_j)Q_{\nu-\frac{1}{2}}(\cosh\tau). \tag{20}$$

Expanding $\cos(\nu(\sigma - \sigma_j))$ and rearranging the terms in Eq. (20) will give

$$\psi_{\text{ring}}(\sigma, \tau) = a_{0,j}T_0(\sigma, \tau) + \sum_{\nu=1}^{\infty}[a_{\nu,j}T_\nu(\sigma, \tau) + b_{\nu,j}U_\nu(\sigma, \tau)] \tag{21}$$

where $a_{\nu,j}$ and $b_{\nu,j}$ are defined as

$$a_{\nu,j} = \frac{q_{\text{ring},j}}{4\pi\varepsilon_0}\frac{\epsilon_\nu}{\pi a}\sqrt{\cosh\tau_j - \cos\sigma_j}\cos(\nu\sigma_j)P_{\nu-\frac{1}{2}}(\cosh\tau_j); \quad \nu = 0, 1, 2\ldots, \tag{22}$$

$$b_{\nu,j} = \frac{q_{\text{ring},j}}{4\pi\varepsilon_0}\frac{\epsilon_\nu}{\pi a}\sqrt{\cosh\tau_j - \cos\sigma_j}\sin(\nu\sigma_j)P_{\nu-\frac{1}{2}}(\cosh\tau_j); \quad \nu = 1, 2, 3\ldots. \tag{23}$$

The potential shown in Eq. (21) is toroidal multipole expansion of potential due to a ring charge located at (σ_j, τ_j) having charge $q_{\text{ring},j}$ on it. Let the number of ring charges used in the BEM be N_{BEM}. Adding the potentials due to all the ring charges, and comparing with the potential shown in Eq. (2) we get toroidal multipole coefficients as follows;

$$a_\nu = \sum_{j=1}^{N_{\text{BEM}}}a_{\nu,j}; \quad \nu = 0, 1, 2, \ldots, \tag{24}$$

$$b_\nu = \sum_{j=1}^{N_{\text{BEM}}}b_{\nu,j}; \quad \nu = 1, 2, 3\ldots. \tag{25}$$

We call this way of computing the multipole coefficients as the Surface Charge BEM (SC-BEM) method. Once a_ν and b_ν are known, we can use the first few terms of Eq. (2) to approximately compute the potential near the trapping circle. It should be noted that the multipole expansion given by Eq. (2) converges only in the region for which $\tau > \max_{1\le j\le N_{\text{BEM}}}\tau_j$. In the toroidal trap this region corresponds to the interior of a constant τ torus.

4.5. Equation of ion motion

In this section we derive the equation of motion in toroidal ion traps. This will be done in order to derive the Mathieu parameters which in turn will be used to estimate secular frequency of ion motion. As pointed out by Higgs and Austin [7] an ion in toroidal ion trap mass analysers can have motion in three independent directions, viz., radial, axial and azimuthal directions. The motion in azimuthal direction is not important for studying oscillatory motion about the trapping circle. In our study we fix $y = 0$ and consider motion in the *xz*-plane. The analysis thus presented provides an idea about the secular frequency of ion motion. For this we need to approximate the potential $\Psi(\sigma, \tau)$ (shown in Eq. (2)) near the point $(a, 0, z_c)$, where the toroidal coordinates (σ, τ) are determined from the Cartesian coordinates $(x, 0, z)$. Now $\Psi(x, z)$ is regarded as a function in two variables. To derive the approximate equation of motion near the trapping circle, we expand $\Psi(x, z)$ as

$$\Psi(x, z) = \Psi(a, z_c) + \begin{bmatrix} x-a & z-z_c \end{bmatrix}\mathbf{g}_\Psi + \frac{1}{2}\begin{bmatrix} x-a & z-z_c \end{bmatrix}\mathbf{H}_\Psi\begin{bmatrix} x-a \\ z-z_c \end{bmatrix} + \ldots \tag{26}$$

where the Taylor series is expanded around a point on trapping circle (a, z_c), $\mathbf{g}_\Psi$ is gradient [29] and $\mathbf{H}_\Psi$ is Hessian [29] of $\Psi(x, z)$ evaluated at the point (a, z_c) respectively. In this series we consider first three terms to obtain equation of ion motion. The Hessian of Ψ is given by $\mathbf{H}_\Psi = \begin{bmatrix} \frac{\partial^2\Psi}{\partial x^2} & \frac{\partial^2\Psi}{\partial z\partial x} \\ \frac{\partial^2\Psi}{\partial x\partial z} & \frac{\partial^2\Psi}{\partial z^2} \end{bmatrix}$. In order to get simplified form of $\mathbf{H}_\Psi$ let us look at the Laplace equation in cylindrical coordinates which is given by $\frac{1}{\rho}\frac{\partial}{\partial\rho}(\rho\frac{\partial\Psi}{\partial\rho}) + \frac{1}{\rho^2}\frac{\partial^2\Psi}{\partial\phi^2} + \frac{\partial^2\Psi}{\partial z^2} = 0$. For axially symmetric geometries the potential Ψ does not depend on ϕ, hence $\frac{\partial^2\Psi}{\partial\phi^2} = 0$. By taking this into account and replacing ρ with x in the Laplace equation we obtain $\frac{\partial^2\Psi}{\partial x^2} + \frac{\partial^2\Psi}{\partial z^2} = 0$ or $\frac{\partial^2\Psi}{\partial z^2} = -\frac{\partial^2\Psi}{\partial x^2}$. Using this along with the relation $\frac{\partial^2\Psi}{\partial z\partial x} = \frac{\partial^2\Psi}{\partial x\partial z}$ we get the

Hessian of Ψ as $\mathbf{H}_\Psi = \begin{bmatrix} u & v \\ v & -u \end{bmatrix}$ where $u = \frac{\partial^2\Psi}{\partial x^2}$ and $v = \frac{\partial^2\Psi}{\partial x \partial z}$. The trace of $\mathbf{H}_\Psi$ is zero and the determinant is $-(u^2+v^2)$. If λ_1 and λ_2 are eigenvalues of $\mathbf{H}_\Psi$ then $\lambda_1+\lambda_2=0$ and $\lambda_1\lambda_2 = -(u^2+v^2)$. So, $\lambda_1 = \sqrt{u^2+v^2}$ and $\lambda_2 = -\lambda_1$. The corresponding eigenvectors are $\begin{bmatrix} \cos\phi \\ \sin\phi \end{bmatrix}$ and $\begin{bmatrix} -\sin\phi \\ \cos\phi \end{bmatrix}$, where ϕ is determined from $\tan\phi = \frac{\sqrt{u^2+v^2}-u}{v} = \frac{v}{\sqrt{u^2+v^2}+u}$. This ensures that the matrix $\mathbf{H}_\Psi$ is diagonalizable and it can be written as

$$\mathbf{H}_\Psi = S^{-1}\begin{bmatrix} \lambda_1 & 0 \\ 0 & \lambda_2 \end{bmatrix} S \tag{27}$$

where S is given by $\begin{bmatrix} \cos\phi & -\sin\phi \\ \sin\phi & \cos\phi \end{bmatrix}$. Next, in order to obtain the equation of motion we need to define the time varying potential. Using the approximate potential given in Eq. (26) we define the time varying potential, $\Phi(x,z,t)$, as

$$\Phi(x,z,t) = [U_{dc} + V_{rf}\cos(\Omega t)]\Psi(x,z) \tag{28}$$

where U_{dc} is d.c. potential, V_{rf} is r.f. potential, Ω is angular frequency of the r.f. drive. Using the time varying potential around the trapping circle we obtain the electric field as

$$-\left[U_{dc} + V_{rf}\cos(\Omega t)\right]\mathbf{H}_\Psi \begin{bmatrix} x-a \\ z-z_c \end{bmatrix}$$

and the equations of motion in x and z direction can be written as

$$\begin{bmatrix} m\frac{d^2x}{dt^2} \\ m\frac{d^2z}{dt^2} \end{bmatrix} = -e\left[U_{dc} + V_{rf}\cos(\Omega t)\right]\mathbf{H}_\Psi \begin{bmatrix} x-a \\ z-z_c \end{bmatrix} \tag{29}$$

where m is mass of the ion, e is charge of the ion. On substitution of $\Omega t = 2\xi$ and $\mathbf{H}_\Psi$ given in Eq. (27), and also assuming

$$\begin{bmatrix} u_1 \\ u_2 \end{bmatrix} = S\begin{bmatrix} x-a \\ z-z_c \end{bmatrix}, \tag{30}$$

Eq. (29) takes the form of Mathieu equation [23]

$$\begin{bmatrix} \frac{d^2u_1}{d\xi^2} \\ \frac{d^2u_2}{d\xi^2} \end{bmatrix} + \begin{bmatrix} \left[a_{Mathieu1} - 2q_{Mathieu1}\cos(2\xi)\right]u_1 \\ \left[a_{Mathieu2} - 2q_{Mathieu2}\cos(2\xi)\right]u_2 \end{bmatrix} = \begin{bmatrix} 0 \\ 0 \end{bmatrix} \tag{31}$$

where

$$a_{Mathieu1} = \frac{4eU_{dc}\lambda_1}{m\Omega^2}, \tag{32}$$

$$q_{Mathieu1} = -\frac{2eV_{rf}\lambda_1}{m\Omega^2}, \tag{33}$$

$$a_{Mathieu2} = \frac{4eU_{dc}\lambda_2}{m\Omega^2} = -a_{Mathieu1}, \tag{34}$$

$$q_{Mathieu2} = -\frac{2eV_{rf}\lambda_2}{m\Omega^2} = -q_{Mathieu1} \tag{35}$$

are Mathieu parameters [1]. It should be noted that the magnitudes of the Mathieu parameters are equal, that is $|a_{Mathieu1}| = |a_{Mathieu2}|$ and $|q_{Mathieu1}| = |q_{Mathieu2}|$. This feature is a similar to that we see for the LIT. This feature of toroidal ion trap is not unexpected, because as the radius of trapping circle tends to infinity, the structure locally resembles that of the LIT. An alternative is to consider a point very close to the trapping circle. Here too the same picture applies.[1] Once we know Mathieu parameters it is straight forward to get frequencies of ion motion from the theory of Mathieu equation [23]. To obtain Mathieu parameters in Eqs. (32)–(35) the unknowns are the eigenvalues of $\mathbf{H}_\Psi$, λ_1 and λ_2. To obtain these eigenvalues we start by making use of the linearity property of Hessian to get

$$\mathbf{H}_\Psi = a_0\mathbf{H}_{T_0} + \sum_{\nu=1}^{\infty}\left[a_\nu\mathbf{H}_{T_\nu} + b_\nu\mathbf{H}_{U_\nu}\right]. \tag{36}$$

We observed that in Eq. (36) $\mathbf{H}_{T_\nu}$, $\mathbf{H}_{U_\nu}$ are zero for $\nu > 2$. Using this, Eq. (36) takes the form

$$\mathbf{H}_\Psi = a_0\mathbf{H}_{T_0} + \sum_{\nu=1}^{2}[a_\nu\mathbf{H}_{T_\nu} + b_\nu\mathbf{H}_{U_\nu}]. \tag{37}$$

From our earlier discussion we already know how to compute a_0, a_1, a_2, b_1 and b_2. Further, it is sufficient to have $\mathbf{H}_{T_\nu}$ for $\nu = 0, 1, 2$ and $\mathbf{H}_{U_\nu}$ for $\nu = 1, 2$ in Eq. (37). Our next focus is to obtain $\mathbf{H}_{T_\nu}$ for $\nu = 0$, 1, 2 and $\mathbf{H}_{U_\nu}$ for $\nu = 1, 2$. To do this, we need to find gradient and Hessian of toroidal harmonics T_0, T_1, T_2, U_1 and U_2 by expressing them in terms of d_1 and d_2 (shown in Fig. 7). T_0, T_1, T_2, U_1 and U_2 in terms of d_1 and d_2 have been derived in Appendix A. The final expressions have the form

$$T_0 = \frac{2a\sqrt{2}}{d_1}K\left(\frac{d_2}{d_1}\right), \tag{38}$$

$$T_1 = \frac{a\sqrt{2}\left(d_1^2+d_2^2-4a^2\right)}{d_1d_2^2}\left[K\left(\frac{d_2}{d_1}\right) - E\left(\frac{d_2}{d_1}\right)\right], \tag{39}$$

$$T_2 = \frac{2\sqrt{2}\,a\left(d_1^2d_2^2 - 8a^2(z-z_c)^2\right)}{3d_1^3d_2^4}\left[(2d_1^2+d_2^2)K\left(\frac{d_2}{d_1}\right) - 2(d_1^2+d_2^2)E\left(\frac{d_2}{d_1}\right)\right], \tag{40}$$

$$U_1 = \frac{4\sqrt{2}a(z-z_c)}{d_1d_2^2}\left[K\left(\frac{d_2}{d_1}\right) - E\left(\frac{d_2}{d_1}\right)\right], \tag{41}$$

$$U_2 = \frac{4\sqrt{2}\,a^2(z-z_c)\left(d_1^2+d_2^2-4a^2\right)}{3d_1^3d_2^4}\left[(2d_1^2+d_2^2)K\left(\frac{d_2}{d_1}\right) - 2(d_1^2+d_2^2)E\left(\frac{d_2}{d_1}\right)\right]. \tag{42}$$

In these expressions $K(.)$ and $E(.)$ are complete elliptic integrals. We express d_1 and d_2 in terms of x, z and substitute these in the respective formulae. From these, we obtain gradient and Hessian for first three toroidal harmonics on the trapping circle. Thus the obtained gradients $\mathbf{g}_{T_\nu}$, $\mathbf{g}_{U_\nu}$ and Hessians $\mathbf{H}_{T_\nu}$, $\mathbf{H}_{U_\nu}$ are shown in Table 2. It is to be noted from Table 2, that first derivative of T_2 and U_2 with respect to x as well as z is zero. It is observed that the first derivative of T_ν and U_ν are zero for $\nu > 1$. Similarly, $\mathbf{H}_{T_\nu}$ and $\mathbf{H}_{U_\nu}$ are zero for $\nu > 2$. The first derivative with respect to x of T_1 is negative half of T_0's derivative with respect to x. The first derivative of linear combination of $a_0T_0 + a_1T_1$ will be zero only when $a_1 = 2a_0$. The derivative of U_1 with respect to z on trapping circle is non zero.

[1] This insight has been provided by the second anonymous reviewer.

Table 2
$\mathbf{g}_{T_\nu}$, $\mathbf{g}_{U_\nu}$, $\mathbf{H}_{T_\nu}$ and $\mathbf{H}_{U_\nu}$ on trapping circle.

	T_0	T_1	T_2	U_1	U_2
$\mathbf{g}$	$\frac{\pi}{a\sqrt{2}}\begin{bmatrix}-\frac{1}{2}\\0\end{bmatrix}$	$\frac{\pi}{a\sqrt{2}}\begin{bmatrix}\frac{1}{4}\\0\end{bmatrix}$	$\begin{bmatrix}0\\0\end{bmatrix}$	$\frac{\pi}{a\sqrt{2}}\begin{bmatrix}0\\\frac{1}{4}\end{bmatrix}$	$\begin{bmatrix}0\\0\end{bmatrix}$
H	$\frac{\pi}{a^2\sqrt{2}}\begin{bmatrix}\frac{5}{8}&0\\0&-\frac{1}{8}\end{bmatrix}$	$\frac{\pi}{a^2\sqrt{2}}\begin{bmatrix}-\frac{1}{2}&0\\0&\frac{1}{4}\end{bmatrix}$	$\frac{\pi}{a^2\sqrt{2}}\begin{bmatrix}\frac{3}{16}&0\\0&-\frac{3}{16}\end{bmatrix}$	$\frac{\pi}{a^2\sqrt{2}}\begin{bmatrix}0&-\frac{3}{8}\\-\frac{3}{8}&0\end{bmatrix}$	$\frac{\pi}{a^2\sqrt{2}}\begin{bmatrix}0&\frac{3}{16}\\\frac{3}{16}&0\end{bmatrix}$

The field at trapping circle will be non zero unless $b_1 = 0$. Taking all these into account we get $\mathbf{H}_\Psi$ on trapping circle as

$$\mathbf{H}_\Psi = \frac{3\pi}{16a^2\sqrt{2}}\begin{bmatrix}-2a_0+a_2 & b_2\\ b_2 & 2a_0-a_2\end{bmatrix}. \tag{43}$$

Finally, the eigenvalues of the matrix $\mathbf{H}_\Psi$, λ_1 and λ_2 which are required for obtaining the Mathieu parameters a_{Mathieu1}, q_{Mathieu1}, a_{Mathieu2} and q_{Mathieu2} are given by

$$\lambda_1 = \frac{3\pi}{16a^2\sqrt{2}}\sqrt{(2a_0-a_2)^2+b_2^2}, \tag{44}$$

$$\lambda_2 = -\lambda_1. \tag{45}$$

Once we know the Mathieu parameters we can compute β_1 [1] from a_{Mathieu1} and q_{Mathieu1}, β_2 from a_{Mathieu2} and q_{Mathieu2}. It is to be noted that the β_1 and β_2 will be the same, as the respective Mathieu parameters have the same magnitude. Hence the angular frequencies $\omega_1 = \beta_1\frac{\Omega}{2}$ and $\omega_2 = \beta_2\frac{\Omega}{2}$ are the same. The matrix $\mathbf{H}_\Psi$ has two orthogonal eigenvectors. The directions along these eigenvectors are the principal directions. Since the secular frequency of oscillation is same in both principal directions, in our numerical trajectory simulations we will focus only on the x-direction frequency. The numerically obtained secular frequency will be compared to the predicted secular frequency obtained from a_{Mathieu1} and q_{Mathieu1}.

5. Results and discussions

In this section we present three broad studies. First of these is the estimation of the toroidal multipole coefficients, obtained by the methods outlined by us, for the five traps discussed in the Section 2, viz., HypTorTrap, CylTorTrap, CircRodTorTrap0, CircRodTorTrap30 and CircRodTorTrap45. The second study will estimate the accuracy of these methods in predicting potentials within these traps. Finally, the secular frequency of ion motion in these traps will be computed numerically and compared with the secular frequency obtained from the Mathieu parameters shown in Section 4.5.

5.1. Toroidal multipole coefficients

We have carried out detailed evaluation of multipole coefficients estimated by the three methods outlined above, viz., LS, DFT and SC-BEM on all the five traps we had presented as example traps in the Section 2.

In all these computations the dimensions of the traps are those reported in Table 1. Also, in all the computations the endcap electrodes are kept at −0.5 V and the ring electrodes are kept at 0.5 V.

In order to determine multipole coefficients using the SC-BEM method we need surface charge distribution. This surface charge distribution is found by the method discussed in Section 3.1. Once the charge distribution is known, we use Eqs. (24) and (25) to obtain the toroidal multipole coefficients a_ν and b_ν, respectively. The computed multipole coefficients are presented against the SC-BEM column in the tables. In order to compute multipole coefficients using the LS method, we use Eq. (6). In this equation we need potentials at n sample points. The sample points are taken on a square grid of 2 mm around trapping center in xz-plane with 0.2 mm spacing between grid points. In the present study n is set at 121 and the points are uniformly spaced along x and z-direction. At each of these points potential is computed using the BEM. As pointed out earlier, other methods such as finite difference method or finite element method (both of which have not been discussed here) could be used. The computed multipole coefficients are presented against the LS column in the tables. In order to compute the multipole coefficients using DFT method we use Eq. (9) for a_ν and Eq. (10) for b_ν. In these equations α_ν and β_ν are computed from $\hat{g}(\nu)$ and are computed using Eq. (15). In which we need G_ν, the DFT of a finite length sequence of potentials g_k ($k = 0, 1, 2 \ldots N_s - 1$) evaluated on constant τ ($=\tau_c$). These potentials are computed using the BEM with $\tau_c = 4$ and $N_s = 64$. The computed multipole coefficients are presented against the DFT column in the tables.

Tables 3–7 present results of our computation. Table 3 presents results for HypTorTrap, Table 4 for CylTorTrap, Table 5 for CircRodTorTrap0, Table 6 for CircRodTorTrap30 and Table 7 for CircRodTorTrap45.

Table 3
Multipole coefficients for HypTorTrap shown in Fig. 1.

ν	SC-BEM		LS		DFT	
	a_ν	b_ν	a_ν	b_ν	a_ν	b_ν
0	−0.10318	0	−0.10318	0	−0.10318	0
1	−0.20636	0	−0.20636	0	−0.20636	0
2	10.23820	0	10.23820	0	10.23820	0
3	30.52093	0	30.52067	0	30.52093	0
4	97.64751	0	97.64944	0	97.64751	0
5	249.77397	0	249.61923	0	249.77397	0

Table 4
Multipole coefficients for CylTorTrap shown in Fig. 2.

ν	SC-BEM		LS		DFT	
	a_ν	b_ν	a_ν	b_ν	a_ν	b_ν
0	−0.02103	0	−0.02103	0	−0.02103	0
1	−0.04205	0	−0.04205	0	−0.04205	0
2	9.33300	0	9.33300	0	9.33300	0
3	26.81873	0	26.81898	0	26.81873	0
4	70.89814	0	70.90006	0	70.89814	0
5	188.20890	0	188.35898	0	188.20890	0

Table 5
Multipole coefficients for CircRodTorTrap0 shown in Fig. 3.

ν	SC-BEM		LS		DFT	
	a_ν	b_ν	a_ν	b_ν	a_ν	b_ν
0	−0.00144	0	−0.00144	0	−0.00144	0
1	−0.00288	0	−0.00288	0	−0.00288	0
2	37.18441	0	37.18441	0	37.18441	0
3	105.57055	0	105.57021	0	105.57055	0
4	219.51020	0	219.51030	0	219.51020	0
5	2.12578	0	1.31248	0	2.12578	0

Table 6
Multipole coefficients for CircRodTorTrap30 shown in Fig. 4.

ν	SC-BEM		LS		DFT	
	a_ν	b_ν	a_ν	b_ν	a_ν	b_ν
0	−0.00072	0	−0.00072	0	−0.00072	0
1	−0.00144	0	−0.00144	0	−0.00144	0
2	18.59247	32.21638	18.59247	32.21638	18.59247	32.21638
3	53.10867	91.64201	53.10899	91.64199	53.10867	91.64201
4	91.38647	179.55487	91.38632	179.55502	91.38647	179.55487
5	511.15835	296.14233	511.91545	296.18144	511.15835	296.14233

Table 7
Multipole coefficients for CircRodTorTrap45 shown in Fig. 5.

ν	SC-BEM		LS		DFT	
	a_ν	b_ν	a_ν	b_ν	a_ν	b_ν
0	0	0	0	0	0	0
1	0	0	0	0	0	0
2	0	37.20045	0	37.20045	0	37.20045
3	0	106.03487	0	106.03518	0	106.03487
4	0	195.07568	0	195.07587	0	195.07568
5	0	682.34054	0	681.61891	0	682.34054

Inspection of these tables indicates that the odd order multipoles b_ν's are all zero for traps having top bottom symmetry. These traps include HypTorTrap, CylTorTrap and CircRodTorTrap0. For other two traps CircRodTorTrap30 and CircRodTorTrap45, which do not have top bottom symmetry odd order multipoles b_ν's are required to describe the field inside the trap.

It can be seen from the tables that these three methods perform well and there is a close match between the multipoles obtained by these methods. We point out that amongst these methods the LS method has marginally larger error. Comparing the LS method and the DFT method, we point out that the DFT method provides computationally more efficient and accurate results.

It should be noted that from Tables 3–7 that the multipole coefficients obtained using the SC-BEM and the DFT are matching till the last digit. This is due to the fact that the potentials used in the DFT are computed using the surface charge distribution obtained from the BEM. In this sense, both techniques rely on the same source data and consequently match so closely.

We also point out that the value for the coefficient a_5 for the trap CircRodTorTrap0 (Table 5) is unusually low when compared to its value for other traps. For a reason we do not understand at this point, this low value appears to be associated with our choice of d= 20 mm. Choosing larger or smaller values for d in these computations, increases the magnitude of a_5. For example, choosing d to be 0.8 times the current value (20 mm) gives a_5 =−136.87188 while choosing it to be 1.2 times the current value results in a_5 becoming 47.39634.

As has been pointed out earlier, for the trapping of ions to occur in these traps the gradient of the potential $\Psi(\sigma, \tau)$ on the trapping circle needs be zero. A condition for this to happen was seen to be $a_1 = 2a_0$ and $b_1 = 0$. An inspection of these tables indicates that this is indeed met. For instance in HypTorTrap (Table 3), a_0 =−0.10318, a_1 =−0.20636 and $b_1 = 0$. Similar conclusions can be reached for other traps too.

5.2. Accuracy of estimating potentials using multipoles

For estimating the accuracy of our method, we compare the potentials obtained using our multipole coefficients (using Eq. (2)) with those obtained numerically using the BEM.

Two studies have been presented here.

In the first, we present a comparison of potential obtained from multipoles with potential obtained using the BEM, for all the traps shown in the Section 2. The BEM potential is computed with −0.5 V on the endcaps and 0.5 V on the ring electrodes. Although these studies have been carried out on all the five traps, we present results for only two traps for the sake of brevity. The first trap has top bottom symmetry, HypTorTrap. Here we choose multipoles a_0, a_1, a_2 and a_3 to obtain the potential. The second trap does not have top bottom symmetry cirRodTorTrap30 and here we choose a_0, a_1, a_2, a_3, b_2 and b_3 multipole coefficients to characterize the potential. We mention in passing that the results of these studies on the other three traps are similar to the results we presented here.

In the second study we present the results of how taking smaller or larger number of multipoles in the expansion of the potential impacts the accuracy of the predicted result.

Fig. 10 shows potential on the circle $\tau = 3$ for the trap HypTorTrap. Fig. 10(a) shows comparison of potential obtained using the multipoles a_0, a_1, a_2 and a_3 with the BEM. There is a good agreement between the potential obtained from multipoles in comparison to the BEM. Fig. 10(b) shows error in the potential obtained using the multipoles in comparison to the BEM, which is of the order of 10^{-4} volts.

Fig. 11 shows potential on the circle $\tau = 3$ for the trap cirRodTorTrap30. Fig. 11(a) shows comparison of potential obtained using the multipoles a_0, a_1, a_2, a_3, b_2 and b_3 with the BEM. There is good agreement between the potential obtained from multipoles in comparison to the BEM. Fig. 11(b) shows error in the potential obtained using the multipoles in comparison to the BEM, which is small in comparison to the potential.

Table 8 shows the results of our studies how our methods predicts the potentials when we take smaller or larger number

Table 8
Maximum absolute error in the potential obtained from multipoles in comparison to the BEM potential on $\tau = 3$ circle.

TRAP	Multipoles	Maximum absolute error (volts)
HypTorTrap	a_0, a_1	0.02299
	a_0, a_1, a_2	0.00288
	a_0, a_1, a_2, a_3	0.00039
	a_0, a_1, a_2, a_3, a_4	0.00004
CylTorTrap	a_0, a_1	0.02080
	a_0, a_1, a_2	0.00247
	a_0, a_1, a_2, a_3	0.00028
	a_0, a_1, a_2, a_3, a_4	0.00003
CircRodTorTrap0	a_0, a_1	0.08243
	a_0, a_1, a_2	0.00940
	a_0, a_1, a_2, a_3	0.00086
	a_0, a_1, a_2, a_3, a_4	0.00001
CircRodTorTrap30	a_0, a_1	0.08168
	a_0, a_1, a_2, b_2	0.00937
	$a_0, a_1, a_2, a_3, b_2, b_3$	0.00082
	$a_0, a_1, a_2, a_3, a_4, b_2, b_3, b_4$	0.00011
CircRodTorTrap45	b_2	0.00938
	b_2, b_3	0.00080
	b_2, b_3, b_4	0.00012

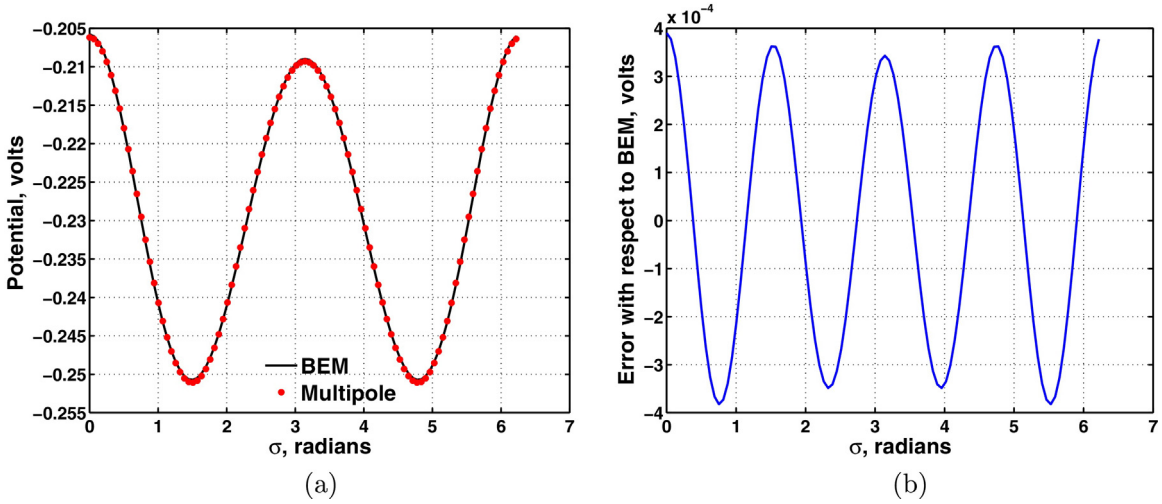

Fig. 10. Potential obtained using the multipoles a_0, a_1, a_2 and a_3 for the trap HypTorTrap. (a) Comparison with the BEM. Potentials obtained from multipoles are marked as (*), and those obtained using the BEM as a smooth curve. (b) Difference of potential obtained by the BEM and that obtained by multipole expansion.

of multipoles to estimate the potential in the trap. In this table the maximum absolute error against each choice of multipole coefficients for different trap is presented.

As can be seen, increasing the number of multipole coefficients to describe the potentials decreases the absolute error. For instance, for hypSymmTorusGeom, considering only two terms gives an absolute error of 0.022 99 V and increasing this number to five terms reduces absolute error to 0.000 04 V. Similar trends can be seen in other traps too.

At this point we have not carried out any detailed investigation on how many multipoles coefficients should be used to best characterize the field within the device.

5.3. Secular frequency

In this section we compare the secular frequency obtained from the Mathieu parameters derived in Eqs. (32) and (33) with the secular frequency obtained from numerical simulations. Two studies have been carried out here. In the first, comparison is carried out at a fixed V_{rf} with $U_{dc} = 0$. In the second we carry out along $U_{dc} = 0$ line for varying V_{rf} in the trap CircRodTorTrap30.

The secular frequency is obtained from the trajectory using "harminv" [43]. The trajectory is computed for 1 ms using Runge-Kutta fourth order method, with step size 10 ns. Initially the ion is kept on x-axis. It is kept, one tenth of distance between ring electrodes away from the trapping point in xz-plane. The initial velocities of the ion are taken to be zero. The electric field required while solving equations of motion to get trajectory, is obtained from boundary element method. The U_{dc} is taken as 0 V, r.f. drive frequency is taken as 1 MHz. The ion considered for simulations has mass to charge ratio 78 Th.

In order to find the secular frequency of ion motion from the theory of Mathieu equation, the Mathieu parameters are computed using equations shown in Eqs. (32) and (33). The eigenvalues of Hessian matrix are computed using Eqs. (44) and (45) which depend on toroidal multipole coefficients a_0, a_2 and b_2. These multipole coefficients are taken from Section 5.1.

The secular frequencies obtained numerically as well as from the Mathieu parameters are shown in Table 9 for all the traps shown in the Section 2. These frequencies are obtained for x-direction motion for mass 78 Th with V_{rf} of 400 V_{0-p}. In this table the secular frequencies shown against the column "Numerical (kHz)" are obtained from numerical trajectory. The predicted secular

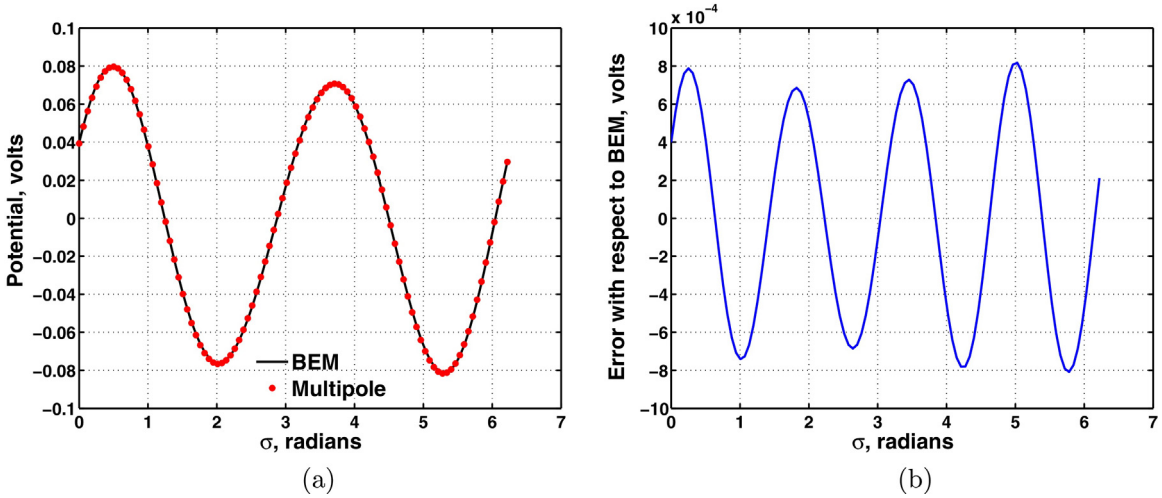

Fig. 11. Potential obtained using the multipoles a_0, a_1, a_2, a_3, b_2 and b_3 for the trap cirRodTorTrap30. (a) Comparison with the BEM. Potentials obtained from multipoles are marked as (*), and those obtained using the BEM as a smooth curve. (b) Difference of potential obtained by the BEM and that obtained by multipole expansion.

Table 9
Secular frequency of mass 78 Th obtained from numerical simulation and predicted using formula for V_{rf} = 400 V.

TRAP	$q_{Mathieu1}$	Numerical (kHz)	Predicted (kHz)	% relative error
HypTorTrap	0.29711	108.90458	106.95137	1.79351
CylTorTrap	0.26626	98.63926	95.49459	3.18806
CircRodTorTrap0	0.24836	89.13224	88.90432	0.25572
CircRodTorTrap30	0.24836	88.95269	88.90274	0.05616
CircRodTorTrap45	0.24835	88.90382	88.90221	0.00182

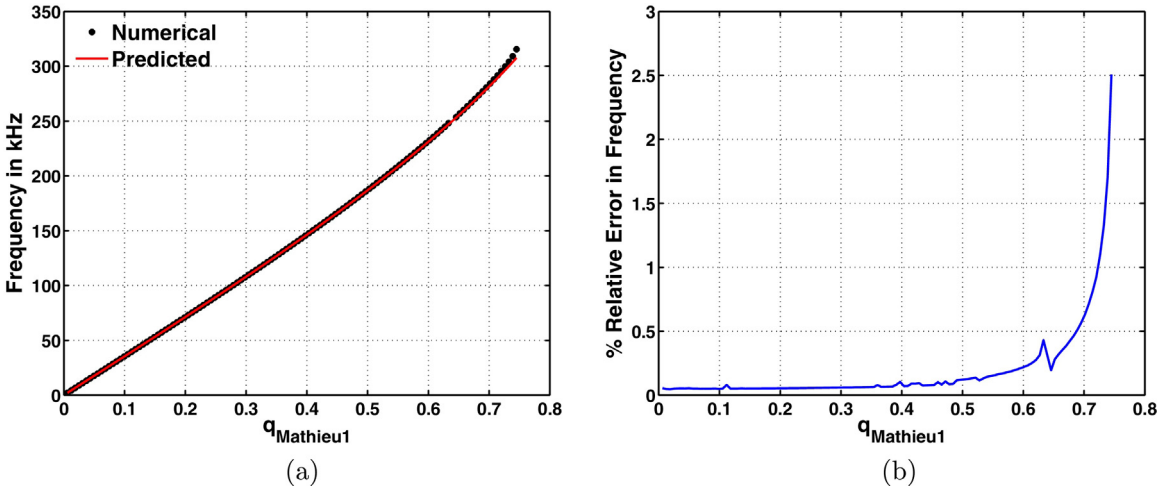

Fig. 12. Predicted secular frequency for the trap CircRodTorTrap30. (a) Comparison with numerical simulation and (b) percentage error in it relative to numerical simulation.

frequencies are obtained from the Mathieu parameters $a_{Mathieu1}$ and $q_{Mathieu1}$ shown in Eqs. (32) and (33). The percentage relative error refers to the error in the predicted frequency relative to the frequency obtained from the numerical trajectory.

It may be noted that there is good match between numerically obtained frequencies and predicted frequencies. Also, the percentage of relative error is reasonably small for all the traps. Further, an inspection of Table 9 indicates that the percentage of relative error varies between 0.00182 for CircRodTorTrap45 to 3.18806 for CylTorTrap. This may be due to differing field nonlinearities in different traps.

Having seen the secular frequency at a fixed V_{rf}, we turn our attention to variation of secular frequency with V_{rf}. The studies include a comparison of secular frequency obtained from our Eqs. (32) and (33) and those obtained numerically and a study which estimates relative error. Although these studies have been carried out on all the traps, we present results only for CircRodTorTrap30 for the sake of brevity. Further, we have this trap because it does not have top bottom symmetry.

Fig. 12 shows secular frequency comparison and relative error with respect to $q_{Mathieu1}$ on $a_{Mathieu1} = 0$ line for CircRodTorTrap30. The secular frequency comparison with respect to $q_{Mathieu1}$ on $a_{Mathieu1} = 0$ line is shown in Fig. 12(a) and relative error is shown in Fig. 12(b).

We point out that there is a gap in Fig. 12(a) at $q_{Mathieu1}$ close to 0.65. The frequencies presented in Fig. 12(a) are only for the stable motion of the ion. The gap in Fig. 12(a) is probably due to nonlinear resonance because nonlinear resonances have been observed in other traps at this q value. Similar gap has been observed for pure toroidal traps by Higgs et al. [8]. These nonlinear resonances also be the cause for larger errors observed near the point of the resonance. This manifests itself as a jump in the error plot shown in Fig. 12(b). Further investigations are required to understand this phenomenon.

6. Concluding remarks

Three different methods have been presented to compute toroidal multipole coefficients. The first method used a least squares fit of the potential around trapping circle with toroidal multipole expansion. In the second method we used discrete Fourier transform of potential. In the third method surface charge distribution has been used to obtain these coefficients.

Using these multipole coefficients we have presented equations of ion motion, the Mathieu parameters in terms of multipole coefficients and the secular frequency of ion motion in these traps.

The accuracy of our method to evaluate multipole coefficients in toroidal ion traps has been demonstrated by the good match that we have obtained for the potentials and secular frequencies obtained by our methods when compared to those obtained numerically.

Acknowledgements

We are grateful to Professor Daniel E. Austin for providing access to Lammert et al. [9]. We thank Professor A.G. Menon for discussions during the preparation of this manuscript. We thank the two anonymous reviewers for their insightful comments which have substantially improved the manuscript.

Appendix A. First few toroidal harmonics in terms of d_1 and d_2

We wish to find first few toroidal harmonics in terms of d_1 and d_2. T_0, T_1, T_2, U_1 and U_2 are obtained from Eqs. (3) and (4) as follows

$$T_0 = \sqrt{\cosh\tau - \cos\sigma}\, Q_{-\frac{1}{2}}(\cosh\tau), \tag{A.1}$$

$$T_1 = \sqrt{\cosh\tau - \cos\sigma}\,\cos\sigma\, Q_{\frac{1}{2}}(\cosh\tau), \tag{A.2}$$

$$T_2 = \sqrt{\cosh\tau - \cos\sigma}\,\cos 2\sigma\, Q_{\frac{3}{2}}(\cosh\tau), \tag{A.3}$$

$$U_1 = \sqrt{\cosh\tau - \cos\sigma}\,\sin\sigma\, Q_{\frac{1}{2}}(\cosh\tau), \tag{A.4}$$

$$U_2 = \sqrt{\cosh\tau - \cos\sigma}\,\sin 2\sigma\, Q_{\frac{3}{2}}(\cosh\tau). \tag{A.5}$$

We see in these expressions that $\cosh\tau$, $\cos\sigma$, $\cos 2\sigma$, $\sin\sigma$ and $\sin 2\sigma$ are needed in terms of d_1 and d_2. From the definition of τ shown in Fig. 7 we get

$$e^{\tau} = \frac{d_1}{d_2}, \tag{A.6}$$

from which we obtain

$$\cosh\tau = \frac{d_1^2 + d_2^2}{2d_1d_2}, \tag{A.7}$$

$\cos\sigma$ and $\sin\sigma$ are obtained from the triangle F_1PF_2 (shown in Fig. 7) by applying cosine and sine rule respectively to give

$$\sin\sigma = \frac{2a(z - z_c)}{d_1d_2}, \tag{A.8}$$

$$\cos\sigma = \frac{d_1^2 + d_2^2 - 4a^2}{2d_1d_2}. \tag{A.9}$$

It is to be noted that once $\cos\sigma$ and $\sin\sigma$ are known we can compute $\cos 2\sigma$ and $\sin 2\sigma$ in terms of d_1 and d_2.

We also see Eqs. (A.1)–(A.5) contain one of $Q_{-\frac{1}{2}}$, $Q_{\frac{1}{2}}$ and $Q_{\frac{3}{2}}$. Formulae for $Q_{-\frac{1}{2}}$ and $Q_{\frac{1}{2}}$ are adapted from the DLMF [38,40,41] as follows

$$Q_{-\frac{1}{2}}(\cosh\tau) = 2e^{-\tau/2}K(e^{-\tau}), \tag{A.10}$$

$$Q_{\frac{1}{2}}(\cosh\tau) = \cosh\tau\,\mathrm{sech}(\frac{1}{2}\tau)K\left(\mathrm{sech}\left(\frac{1}{2}\tau\right)\right) - 2\cosh(\frac{1}{2}\tau)E(\mathrm{sech}(\frac{1}{2}\tau)), \tag{A.11}$$

where $K(.)$ and $E(.)$ are complete elliptic integrals of the first and the second kind respectively [38,39].

Further, $Q_{\frac{1}{2}}(\cosh\tau)$ is simplified by applying the descending Landen transformation [38,42]

$$k' = \sqrt{1 - k^2}, \tag{A.12}$$

$$k_1 = \frac{1 - k'}{1 + k'}, \tag{A.13}$$

$$K(k) = (1 + k_1)K(k_1), \tag{A.14}$$

$$E(k) = (1 + k')E(k_1) - k'K(k), \tag{A.15}$$

on $K(k)$ and $E(k)$ with $k = \mathrm{sech}(\frac{1}{2}\tau)$ to obtain

$$Q_{\frac{1}{2}}(\cosh\tau) = 2e^{\frac{\tau}{2}}\left[K(e^{-\tau}) - E(e^{-\tau})\right]. \tag{A.16}$$

We obtain $Q_{\frac{3}{2}}(\cosh\tau)$ in terms of $Q_{-\frac{1}{2}}$ and $Q_{\frac{1}{2}}$ from the recurrence relation of associated Legendre functions as follows

$$Q_{\frac{3}{2}}(\cosh\tau) = \frac{4}{3}\cosh\tau Q_{\frac{1}{2}}(\cosh\tau) - \frac{1}{3}Q_{-\frac{1}{2}}(\cosh\tau). \tag{A.17}$$

On substitution of e^{τ} from Eq. (A.6), $\cosh\tau$ from (A.7) in Eqs. (A.10), (A.16) and (A.17), we obtain $Q_{-\frac{1}{2}}$, $Q_{\frac{1}{2}}$ and $Q_{\frac{3}{2}}$ in terms of d_1 and d_2 as follows

$$Q_{-\frac{1}{2}}(\cosh\tau) = 2\sqrt{\frac{d_2}{d_1}}K\left(\frac{d_2}{d_1}\right), \tag{A.18}$$

$$Q_{\frac{1}{2}}(\cosh\tau) = 2\sqrt{\frac{d_1}{d_2}}\left[K\left(\frac{d_2}{d_1}\right) - E\left(\frac{d_2}{d_1}\right)\right], \tag{A.19}$$

$$Q_{\frac{3}{2}}(\cosh\tau) = \frac{4}{3}\frac{d_1^2 + d_2^2}{d_1d_2}\sqrt{\frac{d_1}{d_2}}\left[K\left(\frac{d_2}{d_1}\right) - E\left(\frac{d_2}{d_1}\right)\right] - \frac{2}{3}\sqrt{\frac{d_2}{d_1}}K\left(\frac{d_2}{d_1}\right). \tag{A.20}$$

Finally, substitution of $\cosh\tau$, $\cos\sigma$, $\sin\sigma$, $Q_{-\frac{1}{2}}$, $Q_{\frac{1}{2}}$ and $Q_{\frac{3}{2}}$ in terms of d_1 and d_2 in T_0, T_1, T_2, U_1 and U_2 we obtain

$$T_0 = \frac{2a\sqrt{2}}{d_1}K\left(\frac{d_2}{d_1}\right), \tag{A.21}$$

$$T_1 = \frac{a\sqrt{2}\left(d_1^2 + d_2^2 - 4a^2\right)}{d_1d_2^2}\left[K\left(\frac{d_2}{d_1}\right) - E\left(\frac{d_2}{d_1}\right)\right], \tag{A.22}$$

$$T_2 = \frac{2\sqrt{2}\,a\left(d_1^2d_2^2 - 8a^2(z - z_c)^2\right)}{3d_1^3d_2^4}\left[(2d_1^2 + d_2^2)K\left(\frac{d_2}{d_1}\right) - 2(d_1^2 + d_2^2)E\left(\frac{d_2}{d_1}\right)\right], \tag{A.23}$$

$$U_1 = \frac{4\sqrt{2}a(z - z_c)}{d_1d_2^2}\left[K\left(\frac{d_2}{d_1}\right) - E\left(\frac{d_2}{d_1}\right)\right], \tag{A.24}$$

$$U_2 = \frac{4\sqrt{2}\,a^2(z - z_c)\left(d_1^2 + d_2^2 - 4a^2\right)}{3d_1^3d_2^4}\left[(2d_1^2 + d_2^2)K\left(\frac{d_2}{d_1}\right) - 2(d_1^2 + d_2^2)E\left(\frac{d_2}{d_1}\right).\right] \tag{A.25}$$

From these expressions it is possible to obtain the gradient and the Hessian of each of the toroidal harmonics.

References

[1] R.E. March, R.J. Hughes, Quadrupole Storage Mass Spectrometry, Wiley-Interscience, New York, 1989.
[2] I. Waki, S. Kassner, G. Birkl, H. Walther, Observation of ordered structures of laser cooled ions in a quadrupole storage ring, Phys. Rev. Lett. 68 (1992) 2007–2010.
[3] D.A. Church, Storage ring ion trap derived from the linear quadrupole radio frequency mass filter, J. Appl. Phys. 40 (1969) 3127–3134.
[4] M.E. Bier, J.E.P. Syka, Ion Trap Mass Spectrometer System and Method, 1995, U.S. Patent No. 5420425 A.
[5] S.A. Lammert, W.R. Plass, C.V. Thompson, M.B. Wise, Design, optimization and initial performance of a toroidal RF ion trap mass spectrometer, Int. J. Mass Spectrom. 212 (2001) 25–40.
[6] S.A. Lammert, A.A. Rockwood, M. Wang, M.L. Lee, E.D. Lee, S.E. Tolley, J.R. Oliphant, J.L. Jones, R.W. Waite, Miniature toroidal radio frequency ion trap mass analyzer, J. Am. Soc. Mass Spectrom. 17 (2006) 916–922.
[7] J.M. Higgs, D.E. Austin, Simulations of ion motion in toroidal ion traps, Int. J. Mass Spectrom. 363 (2014) 40–51.
[8] J.M. Higgs, B.V. Petersen, S.A. Lammert, K.F. Warnick, D.E. Austin, Radiofrequency trapping of ions in a pure toroidal potential distribution, Int. J. Mass Spectrom. 395 (2016) 20–26.
[9] S. Lammert, E. Lee, R. Waite, J. Oliphant, D. Austin, J. Higgs, K.F. Warnick, D. Tolley, Toroidal multipole expansion for the design of circular ion traps, in: 62nd ASMS Conference on Mass Spectrometry and Allied Topics, 2014.
[10] N. Taylor, D.E. Austin, A simplified toroidal ion trap mass analyzer, Int. J. Mass Spectrom. 321 (2012) 25–32.
[11] M. Wang, H.E. Quist, B.J. Hansen, Y. Peng, Z. Zhang, A.R. Hawkins, A.L. Rockwood, D.E. Austin, M.L. Lee, Performance of a halo ion trap mass analyzer with exit slits for axial ejection, J. Am. Soc. Mass Spectrom. 22 (2011) 369–378.
[12] J.A. Contreras, J.A. Murray, S.E. Tolley, J.L. Oliphant, H.N. Tolley, S.A. Lammert, E.D. Lee, D.W. Later, M.L. Lee, Hand-portable gas chromatograph-toroidal ion trap mass spectrometer (GC-TMS) for detection of hazardous compounds, J. Am. Soc. Mass Spectrom. 19 (2008) 1425–1434.

[13] D.E. Austin, M. Wang, S.E. Tolley, J.D. Maas, A.R. Hawkins, A.L. Rockwood, H.D. Tolley, E.D. Lee, M.L. Lee, Halo Ion Trap Mass Spectrometer, Anal. Chem. 79 (2007) 2927–2932.
[14] M.J. Madsen, C.H. Gorman, Compact toroidal ion-trap design and optimization, Phys. Rev. A 82 (2010) 0434231–0434237.
[15] Y. Peng, B.J. Hansen, H. Quist, Z. Zhang, M. Wang, A.R. Hawkins, D.E. Austin, Coaxial ion trap mass spectrometer: concentric toroidal and quadrupolar trapping regions, Anal. Chem. 83 (2011) 5578–5584.
[16] P.K. Tallapragada, A.K. Mohanty, A. Chatterjee, A.G. Menon, Geometry optimization of axially symmetric ion traps, Int. J. Mass Spectrom. 264 (2007) 38–52.
[17] E.R. Badman, R.C. Johnson, W.R. Plass, R.G. Cooks, A Miniature cylindrical quadrupole ion trap: simulation and experiment, Anal. Chem. 70 (1998) 4896–4901.
[18] G. Wu, R.G. Cooks, Z. Ouyang, Geometry optimization for the cylindrical ion trap: field calculations, simulations and experiments, Int. J. Mass Spectrom. 241 (2005) 119–132.
[19] P.M. Morse, H. Feshbach, Methods of Theoretical Physics, Part I, McGraw-Hill, New York, 1953.
[20] P.M. Morse, H. Feshbach, Methods of Theoretical Physics, Part II, McGraw-Hill, New York, 1953.
[21] E.W. Hobson, The Theory of Spherical and Ellipsoidal Harmonics, Chelsea Publishing Company, New York, 1965.
[22] H.E. Fettis, A new method for computing toroidal harmonics, Math. Comput. 24 (1970) 667–670, Available at: http://www.jstor.org/stable/2004843.
[23] N.W. McLachlan, Theory and Application of Mathieu Functions, Dover, New York, 1962.
[24] K. Atkinson, An Introduction to Numerical Analysis, 2nd ed., John Wiley, New York, 1989.
[25] E. Kreyszig, Advanced Engineering Mathematics, 8th ed., John Wiley, New York, 1999.
[26] E. Brigham, The Fast Fourier Transform and its Applications, 1st ed., Prentice Hall, New Jersey, 1988.
[27] M.J. Ablowitz, A.S. Fokas, Complex Variables: Introduction and Applications, 2 Ed., Cambridge University Press, New York, 2003.
[28] E. Chu, Discrete and Continuous Fourier Transforms: Analysis, Applications and Fast Algorithms, Chapman and Hall/CRC, United Kingdom, 2008.
[29] R. Fletcher, Practical Methods of Optimization, 2nd ed., John Wiley, New York, 2000.
[30] E.C. Beaty, Calculated Electrostatic Properties of Ion Traps, Phys. Rev. A 33 (1986) 3645–3656.
[31] G. Strang, Linear Agebra and Its Applications, 2 Ed., Academic Press Inc., New York, 1980.
[32] P. Bevington, D.K. Robinson, Data Reduction and Error Analysis for the Physical Sciences, 3rd ed., McGraw-Hill, New York, 2002.
[33] C.L. Lawson, R.J. Hanson, Solving Least Squares Problems, Society for Industrial and Applied Mathematics, Philadelphia, 1987.
[34] D.J. Douglas, T.A. Glebova, M. Yu Sudakov, Spatial harmonics of the field in a quadrupole mass filter with circular electrodes, Tech. Phys. 44 (1999) 1215–1219.
[35] A. Krishnaveni, Neeraj Kumar Verma, A.G. Menon, A.K. Mohanty, Numerical observation of preferred directionality in ion ejection from stretched rectilinear ion traps, Int. J. Mass Spectrom. 275 (2008) 11–20.
[36] http://torion.com/products/torion.html.
[37] https://www.math.purdue.edu/wang838/notes/newton.pdf.
[38] http://dlmf.nist.gov/.
[39] http://dlmf.nist.gov/19.2.
[40] http://dlmf.nist.gov/14.3.
[41] http://dlmf.nist.gov/14.5.v.
[42] http://dlmf.nist.gov/19.8.ii.
[43] http://ab-initio.mit.edu/wiki/index.php/Harminv.
[44] https://www.gnu.org/software/octave/.
[45] https://en.wikipedia.org/wiki/Toroidal_coordinates.